

Vortex penetration along twin boundaries in pristine and proton-irradiated FeSe

Original

Vortex penetration along twin boundaries in pristine and proton-irradiated FeSe / Ren, Tong; Sun, Yue; Laviano, Francesco; Sakagami, Ryouzuke; Shi, Zhi Xiang; Tamegai, Tsuyoshi. - In: PHYSICAL REVIEW MATERIALS. - ISSN 2475-9953. - 8:8(2024). [10.1103/physrevmaterials.8.084806]

Availability:

This version is available at: 11583/2995397 since: 2024-12-15T13:35:53Z

Publisher:

American Physical Society

Published

DOI:10.1103/physrevmaterials.8.084806

Terms of use:

This article is made available under terms and conditions as specified in the corresponding bibliographic description in the repository





Publisher copyright

APS postprint/Author's Accepted Manuscript e postprint versione editoriale/Version of Record

This article appeared in PHYSICAL REVIEW MATERIALS, 2024, 8, 8, and may be found at <http://dx.doi.org/10.1103/physrevmaterials.8.084806>. Copyright 2024 American Physical Society

(Article begins on next page)

Vortex penetration along twin boundaries in pristine and proton-irradiated FeSe

Tong Ren ¹, Yue Sun,² Francesco Laviano ³, Ryousuke Sakagami ¹, Zhi Xiang Shi,² and Tsuyoshi Tamegai ¹

¹*Department of Applied Physics, The University of Tokyo, 7-3-1 Hongo, Bunkyo-ku, Tokyo 113-8656, Japan*

²*Department of Physics, Southeast University, Nanjing 21189, China*

³*Department of Applied Science and Technology, Politecnico di Torino, Turin 10129, Italy*



(Received 26 April 2024; revised 5 July 2024; accepted 9 August 2024; published 21 August 2024)

Below $T_s \sim 90$ K, single-crystal FeSe undergoes a structural phase transition coinciding with the emergence of lattice domain boundaries, termed twin boundaries. Polarized-light microscopy validated the presence of twin boundaries in pristine FeSe and indicated the existence of extensive microsized twinning in proton-irradiated FeSe. In twinned FeSe, vortex penetration displays a fractal, mazelike pattern, likely guided by these twin domains. We speculate substantial microtwinning in the proton-irradiation crystals, yet macroscopic twin boundaries persist as primary conduits for vortex motion.

DOI: [10.1103/PhysRevMaterials.8.084806](https://doi.org/10.1103/PhysRevMaterials.8.084806)

I. INTRODUCTION

In numerous experimental scenarios involving iron-based superconductors (IBSs) and cuprates, instances have been reported where spontaneous breaking of symmetry from a C_4 point group to a C_2 occurs within the crystal lattice structure [1–3]. Such distortion in the underlying lattice is commonly interpreted as being accompanied by an electronic nematic order [4–8]. Simultaneous with the lattice symmetry breaking, there emerges a densely populated arrangement of inhomogeneous domains, separated by atomically thin domain walls, known as twin boundaries (TBs). TBs are planar interfaces between alternately orientated lattice domains that span the whole crystal thickness. They have been extensively studied due to their ubiquitous existence in many high-temperature superconductors, and are known to interact with the vortex system.

Upon encountering inhomogeneous domains in the mixed state of superconductors, the motion of invading vortices is disturbed by the TBs, and a simple model of the critical state becomes insufficient to describe the vortex system. In experimental and simulated situations, TBs were sometimes reported to function as barriers that hinder the transverse propagation of vortices, causing inhomogeneous distribution of vortices close to their presence [9–12]. Others, however, implied that TBs are an easier entrance for vortices by identifying a suppressed superconducting gap near them [13–15]. These seemingly contradictory observations, in principle, could be settled by altering the sign of a biquadratic term representing the coupling between superconductivity and an Ising-type nematicity in the Ginzburg-Landau free energy [16]. In this scenario, positive (negative) coupling results in competition (cooperation) of the order parameters of nematicity and superconductivity. While the boosting or suppression effect of superconductivity due to TBs might vary and is subject to interpretation, the effectiveness of providing essential pinning potential and guiding the motion of vortices similar to canals are evident since it has been previously reported for $\text{YBa}_2\text{Cu}_3\text{O}_{7-\delta}$ [17,18], $\text{Ba}(\text{Fe}_{1-x}\text{Co}_x)_2\text{As}_2$ [12,19], and FeSe

[20,21]. FeSe has proved to be an ideal material for research on vortex-TB interactions because of not only its chemical simplicity but also the broad temperature and doping dome on the phase diagram where nematicity and superconductivity coexist. In our recent study, using a simple but effective magneto-optical (MO) imaging technique, we vividly demonstrated TB-guided motion of vortices in an FeSe single crystal [22], opening a gateway for understanding the global vortex dynamics in the presence of TBs. Moreover, notable nucleation of TBs around an artificial defect in $\text{YBa}_2\text{Cu}_3\text{O}_{7-\delta}$ has been documented in Ref. [23]. A laser damage with a surface dimension of several microns creates TBs as long as $10 \mu\text{m}$ in an originally homogeneous area due to internal stress. To reproduce this nucleation on a microscopic scale, we irradiated our FeSe crystals with high-energy protons (H^+), which should hypothetically inflict structural damage of several angstroms. In the present study, we have undertaken a comprehensive investigation of the interplay between vortices and TBs, as well as the interaction between TBs and artificial defects.

II. EXPERIMENTAL METHODS

Single crystals of FeSe were grown by a vapor transport method similar to the one described in Ref. [24]. The crystals undergo a superconducting transition at ~ 9 K as reported in our previous publications [25–28]. In order to introduce extra point defects, a series of crystals were exposed to 3-MeV proton beams at the Heavy Ion Medical Accelerator (HIMAC), in the National Institute of Radiological Sciences, Chiba. The thickness of these FeSe crystals was cleaved to below $\sim 20 \mu\text{m}$, which is less than half of the projected range of 3-MeV protons, calculated by Stopping and Range of Ions in Matter (SRIM). The crystals were thereafter mounted perpendicularly to the beamline, and exposed to a particle density fluence up to $0.1 \times 10^{16} \text{H}^+/\text{cm}^2$.

Vortex penetration in those crystals was mapped using differential MO imaging, where a background image was subtracted from the original integrated image [29,30]. The

induction resolution of the image is ~ 0.1 G as is described in detail in our previous publications [31,32]. Utilizing birefringence within the orthorhombic state of FeSe, polarized-light microscope imaging was conducted to detect potential TBs on all crystals. To achieve maximum intensity contrast, the analyzer was adjusted to nearly 90° from the polarizer, and the incident polarization was maintained at a 45° angle relative to the orthorhombic lattice axes.

III. RESULTS AND DISCUSSION

A series of polarized-light microscope images of pristine and proton-irradiated FeSe crystals is presented in Figs. 1(a)–1(d). For pristine FeSe, the same surface below and above T_s is contrasted in Figs. 1(a) and 1(b), respectively. The finest twin domains resolved in this crystal have a dimension of $d_{\text{avg}} = 1.2$ μm , as shown in Fig. 1(e). This is narrower than those in BaFe_2As_2 (4–10 μm) [2,31] and underdoped $\text{Ba}(\text{Fe}_{1-x}\text{Co}_x)_2\text{As}_2$ (3 μm) [33]. The spacing between twin domains remains approximately consistent within a given system but varies among different systems due to the square-root law

$$T_w \propto \sqrt{\gamma_{\text{tw}}G}, \quad (1)$$

where T_w represents the average spacing, G denotes the colony size, and γ_{tw} signifies the material-dependent twin boundary energy per unit area. This relationship has been derived from multiple sources (e.g., Ref. [34]). Upon irradiating 0.01×10^{16} H^+/cm^2 protons, more than 10^6 point defects per μm^2 are introduced into the crystal. Direct imaging by high-angle annular dark field scanning transmission electron microscopy (STEM-HAADF) of such nanoscale defects in $\text{FeSe}_{0.5}\text{Te}_{0.5}$ thin films has been documented in Ref. [35]. In FeSe, these nanometer-scale defects will presumably initiate the nucleation of TBs. Figure 1(c) presents an FeSe crystal irradiated with 0.01×10^{16} H^+/cm^2 . In the pristine FeSe, twin domains are either vertical or horizontal and seldom cross to each other. In contrast to that, twin domains in the irradiated crystal are prone to interweaving when colliding from orthogonal directions [domains that are seemingly crossing each other abide by different orientations, e.g., tracked by dashed lines in Fig. 1(c)]. On top of that, some of these twin domains appear to be much broader than those before irradiation. In Fig. 1(c) the wavelength of the modulation varies from 2 to 10 μm [see Fig. 1(f)]. In Fig. 1(d), as irradiation dose increases to 0.1×10^{16} H^+/cm^2 , the wavelength varies in a broader range, sometimes as bulky as tens of microns [vertical dashed lines in Fig. 1(d)]. This is contradictory to the observation in $\text{Ba}(\text{Fe}_{1-x}\text{Co}_x)_2\text{As}_2$ in Ref. [33] where twin domains typically form finer and denser arrays with increasing number of point defects. A justifiable consideration of such an occurrence would be regarding those broader ones as not single twin domains but bundles of submicron-sized domains that are beyond the spatial resolution of our microscope. TBs separating these microdomains nucleate from point defects like they did from a laser-damaged defect as observed in Ref. [23]. Similar situations have been reported in a near-optimally doped $\text{Ba}(\text{Fe}_{1-x}\text{Co}_x)_2\text{As}_2$ crystal [33], and an underdoped $(\text{Ba}_{1-x}\text{Rb}_x)\text{Fe}_2\text{As}_2$ [31].

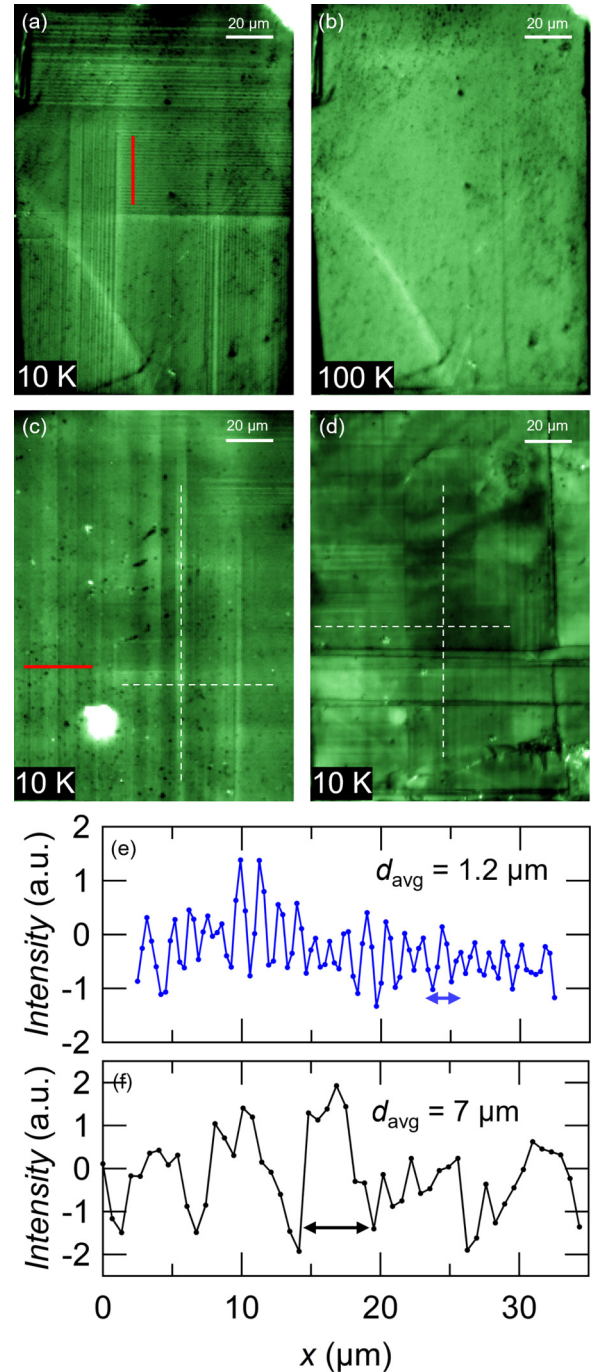


FIG. 1. Polarized-light microscope images of pristine FeSe (a) below and (b) above $T_s \sim 90$ K, and proton-irradiated FeSe with particle density fluence (c) 0.01×10^{16} H^+/cm^2 and (d) 0.1×10^{16} H^+/cm^2 . All images were resolved at 10 K, and are magnified to display the identical scale. White dashed lines are guided to the eye, indicating microdomain bundles that are beyond the resolution limit of ~ 1 μm . Intensity modulation due to twin domains in (e) pristine and (f) 0.01×10^{16} H^+/cm^2 proton-irradiated crystals extracted from the red lines in (a) and (c), respectively.

In order to investigate the behavior of vortices within these crystals, we present the field-dependent critical current density (J_c) in Fig. 2. Additionally, the irradiation dose

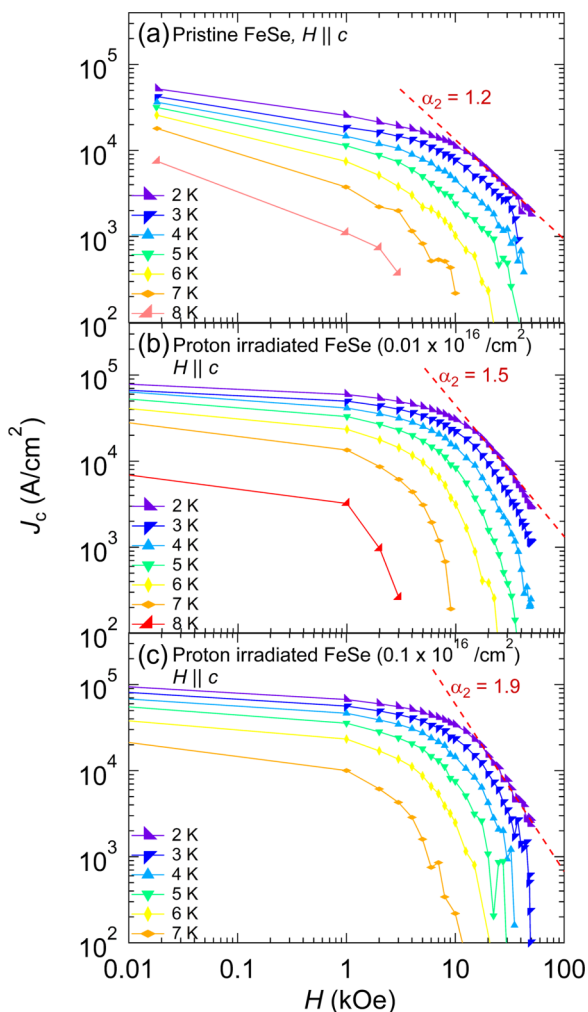


FIG. 2. Magnetic-field-dependent J_c of (a) pristine and [(b), (c)] proton-irradiated FeSe crystals with doses of $0.01 \times 10^{16} \text{ H}^+/\text{cm}^2$ and $0.1 \times 10^{16} \text{ H}^+/\text{cm}^2$, respectively. Dashed lines indicate the power-law fittings.

dependence of T_c is depicted in Fig. 3. Compared with the former findings [36], the T_c -dose diagram demonstrates a notable level of coherence, while J_c in the pristine FeSe [see Fig. 2(a)] decays noticeably more sharply below 1 kOe [25,26]. The rapid decay of J_c at low fields reflects a reduced relaxation rate near the self-field, where the single-vortex creep regime is likely interrupted by the presence of natural defects. It has been reported that J_c follows a power-law decay ($J_c \propto H^{-\alpha}$) at intermediate fields in various kinds of IBSs with α close to $5/8$ [37–39], corresponding to pinning by sparse strong pinning centers [40]. In our previous study, we identified a similar power-law decay of J_c with $\alpha_1 = 0.3\text{--}0.5$ below 10 kOe in both pristine and irradiated FeSe [26]. However, considering the fact that the slopes of J_c - H curves below 10 kOe for FeSe samples shown in Figs. 2(a)–2(c) all change continuously, we cannot define reliable values of α_1 . On the other hand, we find a certain degree of linearity in J_c - H curves above 10 kOe, particularly in the low-temperature regime of pristine FeSe and at the lowest temperatures for irradiated FeSe. We define the slope of J_c - H curves above 10 kOe as α_2 , which is ~ 1.2

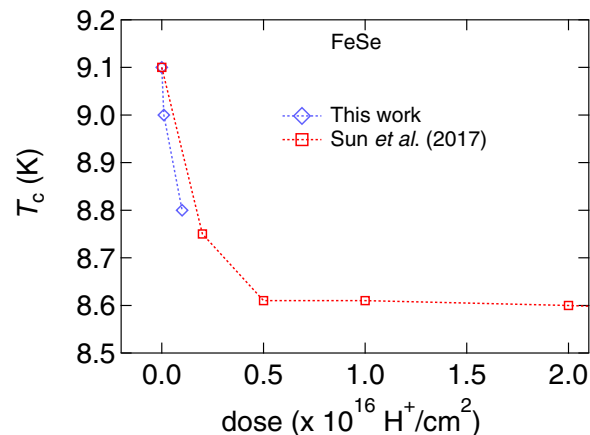


FIG. 3. Relationship between irradiation dose and T_c . Data from the previous study [36] are plotted for comparison.

in the pristine FeSe. TBs as intrinsic pinning centers might be responsible for this large value of α_2 . Since TB arrays are less dense than other strong pinning centers like point defects, they are easily occupied by vortices, leading to a constant pinning force density at high fields and $J_c \propto H^{-1}$. After proton irradiation, J_c (2 K and self-field) was enhanced in a surprising ratio, capped by a factor of 1.6 after $0.1 \times 10^{16} \text{ H}^+/\text{cm}^2$ irradiation, which compares reasonably well with the value reported in Ref. [26], where J_c was enhanced by a factor of 2.7 after $5 \times 10^{16} \text{ H}^+/\text{cm}^2$. The large value of α_2 is also in good alignment with our former findings, except for the unexpected increase after the introduction of point defects. In Figs. 2(b) and 2(c), α_2 seems to scale monotonically with irradiation dose, whereas in Ref. [26] the same material exhibits a nearly constant α_2 after $5 \times 10^{16} \text{ H}^+/\text{cm}^2$ irradiation. To resolve this paradox, we assume there exists a certain degree of competition between TBs and point defects in terms of contributions to the global pinning force. Even with a relatively small dose of irradiation, substantial nucleation of micro-TBs occurs, as we have identified through polarized-light microscopy. These micro-TBs provide a dominant volume fraction of pinning centers compared to point defects (notice that this statement is evidenced by a disproportional enhancement in J_c with merely $1/50$ of irradiation dose compared to Ref. [26]), and α_2 at high magnetic fields reflects a pinning mechanism due to micro-TBs. As the irradiation dose rises, point defects become denser and denser. However, the nucleation of micro-TBs could instead become restrained due to narrower space between point defects. The volume fraction of point defects therefore surpasses micro-TBs at higher irradiation doses, causing α_2 to compromise to the pinning mechanism of point defects. Alternatively, we may need to consider the effect of vortex creep. It has been reported that the normalized relaxation rate $S = |d \ln M/d \ln t|$ strongly increases above certain fields even at low temperatures [25,26]. Such a strong increase in S can make the field dependence of J_c stronger, leading to anomalously large α_2 values with approaching the irreversibility field (H_{irr}). It should be noted that H_{irr} for a pristine FeSe for the $H \parallel c$ axis is reported to be only 120 kOe at $T \sim 2.0 \text{ K}$ [41].

Next, we undertake the investigation into vortex penetration in the aforementioned pristine and proton-irradiated FeSe

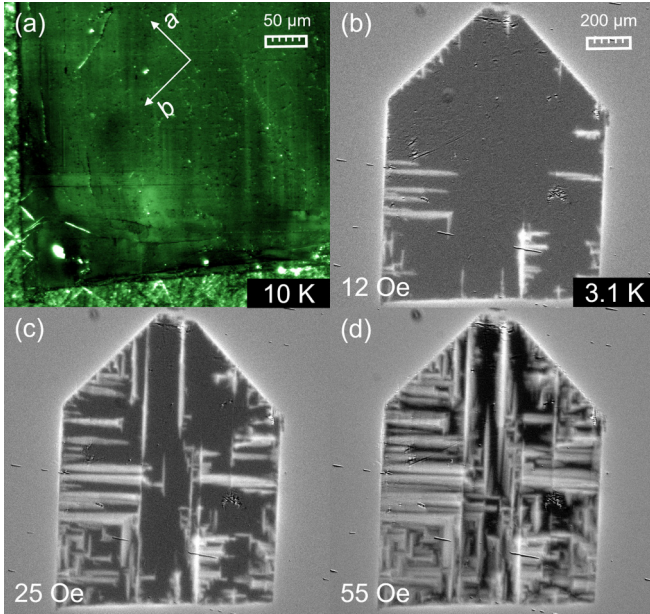


FIG. 4. (a) Polarized-light microscope image focusing on the left bottom corner of a pristine FeSe crystal, which is prepared in a special shape with two edges running along the $a(b)$ axis in the orthorhombic phase. MO images of the same crystal under a ramping magnetic field at (b) 12 Oe, (c) 25 Oe, and (d) 55 Oe after cooling to 3.1 K without field.

crystals utilizing MO imaging. A pristine crystal was shaped into a special house shape by a razor blade. A polarized-light microscope image taken at 10 K presented in Fig. 4(a) exhibits TBs running through the crystal. The full image of this crystal and a more distinct look at TBs in another house-shaped crystal can be found in the Supplemental Material [42]. The bottom and side edges are close to natural edges so that they are either parallel or perpendicular to TBs, while the “rooftops” are cut along the lattice axis in its orthorhombic phase [ab basis in Fig. 4(a)] so that they run along 45° from the TBs. The difference in angles turns out to be critical for the penetration of vortices. In Fig. 4(b), penetration from the bottom and side edges appears to channel along linear defects, indicating the presence of weak links compared to the surrounding bulk. As the magnetic field is increased, the penetration starts to repetitively branch out from the original canals, forming mazelike fractal patterns. The vortex canals are effectively blocked by each other as shown in Figs. 4(c) and 4(d), implying the linear defects also act as strong barriers for the transverse motion of vortices. This barrier effect is more pronounced at the rooftop, where the average penetration of vortices is visibly retarded [see Fig. 4(b)] due to TBs indistinguishably being 45° barriers for the transverse motion of all vortices from the slanted edges. These observations are in excellent agreement with the penetration of vortices observed near TBs in Refs. [12,15], and reproduce the results observed in Ref. [18], where an $\text{YBa}_2\text{Cu}_3\text{O}_{7-\delta}$ crystal was prepared in a similar condition.

We proceed to analyze the proton-irradiated FeSe crystal which has a more complicated, interweaving twinning pattern. A fair reference to this system would be the $\text{YBa}_2\text{Cu}_3\text{O}_{7-\delta}$ thin films which are grown on substrates typi-

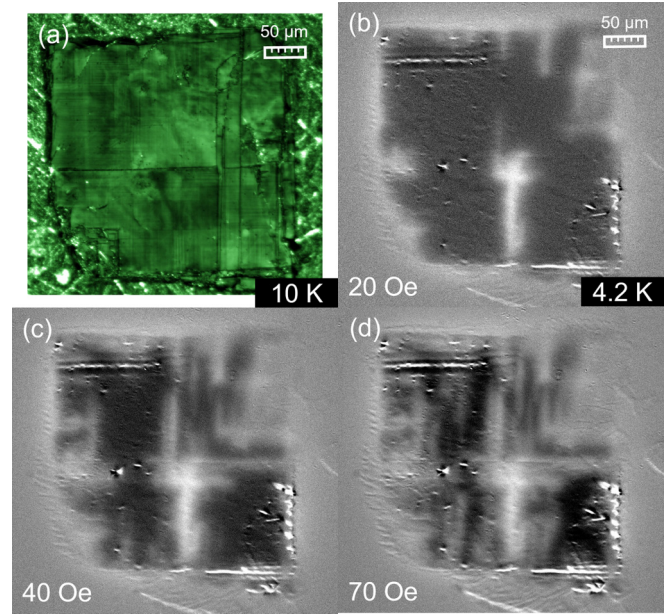


FIG. 5. (a) Polarized-light microscopy image of a proton-irradiated FeSe crystal ($0.1 \times 10^{16} \text{ H}^+/\text{cm}^2$). MO images of vortex penetration in the same crystal under a ramping magnetic field at (b) 20 Oe, (c) 40 Oe, and (d) 70 Oe after cooling to 4.2 K without field.

cally with lattice mismatch. The substantial stress originating from substrate-film interaction leads to dislocations and twinning on a nanometer scale [43,44]. The microtwinning in $\text{YBa}_2\text{Cu}_3\text{O}_{7-\delta}$ thin films is ubiquitous, with only a few exceptions [45]. Despite being heavily microtwinning, MO images of $\text{YBa}_2\text{Cu}_3\text{O}_{7-\delta}$ thin films display a rather homogeneous critical current distribution as reported in Refs. [46,47], distinct from the single crystals, where TBs induce notable inhomogeneities [17,18].

MO images of a proton-irradiated ($0.1 \times 10^{16} \text{ H}^+/\text{cm}^2$) FeSe crystal are presented in Fig. 5. An example of underlining TBs at 10 K is shown in Fig. 5(a). As is described in Fig. 1(d), the modulation of twin domains in this crystal exhibits a rather uneven wavelength and an interweaving pattern. Still, the characteristic mazelike penetration pattern remains without losing any degree of complexity in its fractal nature compared with the pristine FeSe. This finding prompts an argument that, besides the crisscrossing micro-TBs, there are still an essential number of macroscopic TBs that nucleate normally below T_s , and continue to govern the vortex dynamics within this system, primarily acting as conduits or barriers for vortex motions. This assumption redirects our focus to the discussion surrounding Fig. 1. As previously mentioned, the dimensions of modulations due to twin domains in all three crystals vary within certain ranges. Although the nucleation of microtwin domain bundles certainly gives the appearance of bulkiness, selectively sampling from areas with the smallest resolvable modulations [see Figs. 6(a) and 6(b)] reveals that the minimal resolvable dimensions of modulations are nearly identical among all three crystals, as depicted in Figs. 6(c) and 6(d) and in Fig. 1(e). We believe that this minimal modulation reflects the dimension of a typical macroscopic twin

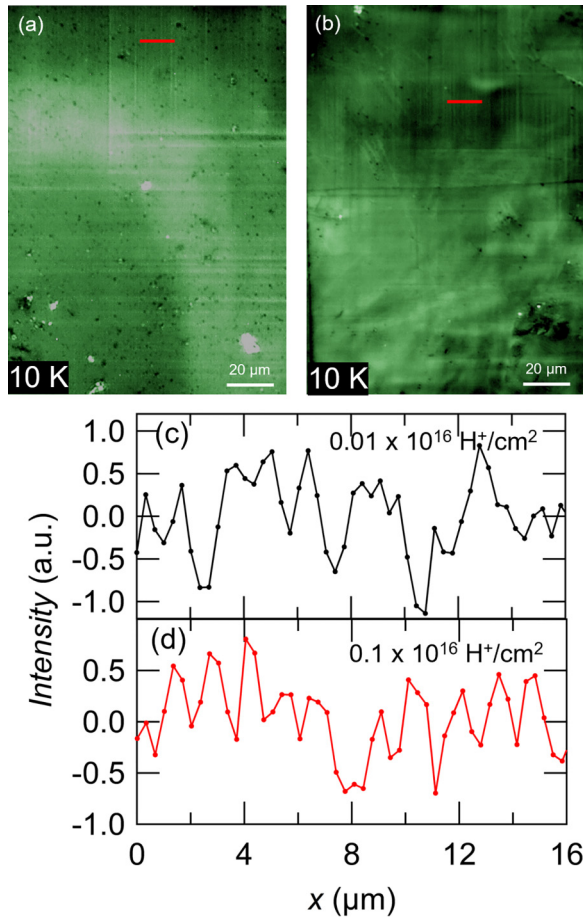


FIG. 6. Polarized-light microscopy image of a difference area (a) in the identical crystals in Fig. 1(c) and 1(b) in Fig. 1(d). Full images of these crystals can be found in the Supplemental Material [42]. Intensity profiles sampled from red lines in (a) and (b), indicating the smallest resolvable modulation in (c) $0.01 \times 10^{16} \text{ H}^+/\text{cm}^2$ and (d) $0.1 \times 10^{16} \text{ H}^+/\text{cm}^2$ irradiated FeSe crystals, respectively.

domain, which is responsible for the fractal-like penetration

pattern in irradiated FeSe crystals as long as the density of the introduced point defects is not too high.

Last but not least, this irradiated sample shares the same thickness of $\sim 10 \mu\text{m}$ with the pristine one in Fig. 4, and the MO imaging was performed at temperatures closer to its T_c . Still, the global penetration of vortices is remarkably retarded. Under 20 Oe, the deepest penetration in the irradiated FeSe is $\sim 100 \mu\text{m}$ [Fig. 5(b)], while in the pristine FeSe, vortices have propagated as deep as $300 \mu\text{m}$ under 12 Oe [Fig. 4(b)]. This retardation is due to higher critical current density after the introduction of point defects by proton irradiation [48].

IV. SUMMARY

Mazelike penetration patterns of vortices in FeSe single crystals were observed via magneto-optical imaging. The motion of vortices appears to be guided and obstructed by the bidirectional twin boundaries, present in both pristine and 3-MeV proton-irradiated FeSe. Variation in the power-law decay factor α of J_c with the magnetic field indicates successful introduction of pointlike defects by proton irradiation. Even at a very small dose of $0.01 \times 10^{16} \text{ H}^+/\text{cm}^2$, J_c in proton-irradiated FeSe crystals was enhanced significantly. This is attributed to the extra pinning centers provided by micro-TBs, whose presence was inferred through polarized-light microscopy. Additionally, although point defects could initiate nucleation of micro-TBs resembling those in $\text{YBa}_2\text{Cu}_3\text{O}_{7-\delta}$ thin films, macroscopic TBs persist and remain largely unchanged in scale, exerting continued dominance over vortex motion.

ACKNOWLEDGMENTS

This work is supported by a Grant in Aid for Scientific Research (A) (Grant No. 17H01141) from the Japan Society of Science (JSPS), and Support for Pioneering Research Initiated by Next Generation (SPRING) of the Japan Science and Technology Agency (JST). Magnetic measurements using a SQUID magnetometer were partly performed using facilities of the Cryogenic Research Center at the University of Tokyo.

- [1] Y. Xu, M. Suenaga, J. Taftø, R. L. Sabatini, A. R. Moodenbaugh, and P. Zolliker, Microstructure, lattice parameters, and superconductivity of $\text{YBa}_2(\text{Cu}_{1-x}\text{Fe}_x)_3\text{O}_{7-\delta}$ for $0 \leq x \leq 0.33$, *Phys. Rev. B* **39**, 6667 (1989).
- [2] M. A. Tanatar, A. Kreyssig, S. Nandi, N. Ni, S. L. Bud'ko, P. C. Canfield, A. I. Goldman, and R. Prozorov, Direct imaging of the structural domains in the iron pnictides AFe_2As_2 ($A = \text{Ca}, \text{Sr}, \text{Ba}$), *Phys. Rev. B* **79**, 180508(R) (2009).
- [3] T. M. McQueen, A. J. Williams, P. W. Stephens, J. Tao, Y. Zhu, V. Ksenofontov, F. Casper, C. Felser, and R. J. Cava, Tetragonal-to-orthorhombic structural phase transition at 90 K in the superconductor $\text{Fe}_{1.01}\text{Se}$, *Phys. Rev. Lett.* **103**, 057002 (2009).
- [4] M. Yi, D. Lu, J. Chu, J. G. Analytis, A. P. Sorini, A. F. Kemper, B. Moritz, S. Mo, R. G. Moore, M. Hashimoto, W. Lee, Z. Hussain, T. P. Devereaux, I. R. Fisher, and Z. Shen, Symmetry-breaking orbital anisotropy observed for detwinned $\text{Ba}(\text{Fe}_{1-x}\text{Co}_x)_2\text{As}_2$ above the spin density wave transition, *Proc. Natl. Acad. Sci. USA* **108**, 6878 (2011).
- [5] T. Sonobe, T. Shimojima, A. Nakamura, M. Nakajima, S. Uchida, K. Kihou, C. H. Lee, A. Iyo, H. Eisaki, K. Ohgushi, and K. Ishizaka, Orbital-anisotropic electronic structure in the nonmagnetic state of $\text{BaFe}_2(\text{As}_{1-x}\text{P}_x)_2$ superconductors, *Sci. Rep.* **8**, 2169 (2018).
- [6] T. Shimojima, Y. Motoyui, T. Taniuchi, C. Bareille, S. Onari, H. Kontani, M. Nakajima, S. Kasahara, T. Shibauchi, Y. Matsuda, and S. Shin, Discovery of mesoscopic nematicity wave in iron-based superconductors, *Science* **373**, 1122 (2021).
- [7] J. Schmidt, V. Bekeris, G. S. Lozano, M. V. Bortulé, M. M. Bermúdez, C. W. Hicks, P. C. Canfield, E. Fradkin, and G. Pasquini, Nematicity in the superconducting mixed state of

- strain detwinned underdoped $\text{Ba}(\text{Fe}_{1-x}\text{Co}_x)_2\text{As}_2$, *Phys. Rev. B* **99**, 064515 (2019).
- [8] F. Yang, S. F. Taylor, S. D. Edkins, J. C. Palmstrom, I. R. Fisher, and B. L. Lev, Nematic transitions in iron pnictide superconductors imaged with a quantum gas, *Nat. Phys.* **16**, 514 (2020).
- [9] G. Crabtree, G. Leaf, H. Kaper, V. Vinokur, A. Koshelev, D. Braun, D. Levine, W. Kwok, and J. Fendrich, Time-dependent Ginzburg-Landau simulations of vortex guidance by twin boundaries, *Physica C (Amsterdam, Neth.)* **263**, 401 (1996).
- [10] W. K. Kwok, J. A. Fendrich, V. M. Vinokur, A. E. Koshelev, and G. W. Crabtree, Vortex shear modulus and lattice melting in twin boundary channels of $\text{YBa}_2\text{Cu}_3\text{O}_{7-\delta}$, *Phys. Rev. Lett.* **76**, 4596 (1996).
- [11] J. A. Herbsommer, G. Nieva, and J. Luzuriaga, Interplay between pinning energy and vortex interaction in $\text{YBa}_2\text{Cu}_3\text{O}_{7-\delta}$ with oriented twin boundaries in tilted magnetic fields: Bitter decoration and tilt-modulus measurements, *Phys. Rev. B* **62**, 3534 (2000).
- [12] B. Kalisky, J. R. Kirtley, J. G. Analytis, J.-H. Chu, I. R. Fisher, and K. A. Moler, Behavior of vortices near twin boundaries in underdoped $\text{Ba}(\text{Fe}_{1-x}\text{Co}_x)_2\text{As}_2$, *Phys. Rev. B* **83**, 064511 (2011).
- [13] C. L. Song, Y. L. Wang, P. Cheng, Y. P. Jiang, W. Li, T. Zhang, Z. Li, K. He, L. Wang, J. F. Jia, H. H. Hung, C. Jun Wu, X. Cun Ma, X. Chen, and Q. K. Xue, Direct observation of nodes and twofold symmetry in FeSe superconductor, *Science* **332**, 1410 (2011).
- [14] C. L. Song, Y. L. Wang, Y. P. Jiang, L. I. Wang, K. He, X. Chen, J. E. Hoffman, X. C. Ma, and Q. K. Xue, Suppression of superconductivity by twin boundaries in FeSe, *Phys. Rev. Lett.* **109**, 137004 (2012).
- [15] I. P. Zhang, J. C. Palmstrom, H. Noad, L. Bishop-Van Horn, Y. Iguchi, Z. Cui, E. Mueller, J. R. Kirtley, I. R. Fisher, and K. A. Moler, Imaging anisotropic vortex dynamics in FeSe, *Phys. Rev. B* **100**, 024514 (2019).
- [16] R. S. Severino, P. D. Mininni, E. Fradkin, V. Bekeris, G. Pasquini, and G. S. Lozano, Ginzburg-Landau approach to the vortex-domain wall interaction in superconductors with nematic order, *Phys. Rev. B* **109**, 094513 (2024).
- [17] V. K. Vlasko-Vlasov, L. A. Dorosinskii, A. A. Polyanskii, V. I. Nikitenko, U. Welp, B. W. Veal, and G. W. Crabtree, Study of the influence of individual twin boundaries on the magnetic flux penetration in $\text{YBa}_2\text{Cu}_3\text{O}_{7-\delta}$, *Phys. Rev. Lett.* **72**, 3246 (1994).
- [18] U. Welp, T. Gardiner, D. Gunter, J. Fendrich, G. Crabtree, V. Vlasko-Vlasov, and V. Nikitenko, Magneto-optical study of twin boundary pinning in $\text{YBa}_2\text{Cu}_3\text{O}_{7-\delta}$, *Physica C (Amsterdam, Neth.)* **235-240**, 241 (1994).
- [19] A. Yagil, Y. Lamhot, A. Almoalem, S. Kasahara, T. Watashige, T. Shibauchi, Y. Matsuda, and O. M. Auslaender, Diamagnetic vortex barrier stripes in underdoped $\text{Ba}(\text{Fe}_{1-x}\text{Co}_x)_2\text{As}_2$, *Phys. Rev. B* **94**, 064510 (2016).
- [20] T. Watashige, Y. Tsutsumi, T. Hanaguri, Y. Kohsaka, S. Kasahara, A. Furusaki, M. Sigrist, C. Meingast, T. Wolf, H. v. Löhneysen, T. Shibauchi, and Y. Matsuda, Evidence for time-reversal symmetry breaking of the superconducting state near twin-boundary interfaces in FeSe revealed by scanning tunneling spectroscopy, *Phys. Rev. X* **5**, 031022 (2015).
- [21] M. L. Amigó, N. Haberkorn, P. Pérez, S. Suárez, and G. Nieva, Vortex dynamics in β -FeSe single crystals: Effects of proton irradiation and small inhomogeneous stress, *Supercond. Sci. Technol.* **30**, 125017 (2017).
- [22] T. Ren, Y. Sun, S. Pyon, and T. Tamegai, Turbulent structure and characterization of '11'-type iron-based superconductors by magneto-optical imaging, *J. Phys.: Conf. Ser.* **2545**, 012006 (2023).
- [23] D. E. Batova, V. K. Vlasko-Vlasov, V. Goncharov, G. A. Emel'chenko, M. V. Indenbom, and Y. A. Osip'yan, Optical polarization contrast and twin-domain structure of high-temperature superconductor single crystals, *Zh. Eksp. Teor. Fiz.* **94**, 356 (1988) [*Sov. Phys. JETP* **67**, 2376 (1988)].
- [24] A. E. Böhmer, F. Hardy, F. Eilers, D. Ernst, P. Adelman, P. Schweiss, T. Wolf, and C. Meingast, Lack of coupling between superconductivity and orthorhombic distortion in stoichiometric single-crystalline FeSe, *Phys. Rev. B* **87**, 180505(R) (2013).
- [25] Y. Sun, S. Pyon, T. Tamegai, R. Kobayashi, T. Watashige, S. Kasahara, Y. Matsuda, and T. Shibauchi, Critical current density, vortex dynamics, and phase diagram of single-crystal FeSe, *Phys. Rev. B* **92**, 144509 (2015).
- [26] Y. Sun, S. Pyon, T. Tamegai, R. Kobayashi, T. Watashige, S. Kasahara, Y. Matsuda, T. Shibauchi, and H. Kitamura, Enhancement of critical current density and mechanism of vortex pinning in H⁺-irradiated FeSe single crystal, *Appl. Phys. Express* **8**, 113102 (2015).
- [27] Y. Sun, S. Pyon, and T. Tamegai, Electron carriers with possible Dirac-cone-like dispersion in $\text{FeSe}_{1-x}\text{S}_x$ ($x = 0$ and 0.14) single crystals triggered by structural transition, *Phys. Rev. B* **93**, 104502 (2016).
- [28] Y. Sun, A. Park, S. Pyon, T. Tamegai, T. Kambara, and A. Ichinose, Effects of heavy-ion irradiation on FeSe, *Phys. Rev. B* **95**, 104514 (2017).
- [29] A. Soibel, E. Zeldov, M. Rappaport, Y. Myasoedov, T. Tamegai, S. Ooi, M. Konczykowski, and V. B. Geshkenbein, Imaging the vortex-lattice melting process in the presence of disorder, *Nature (London)* **406**, 282 (2000).
- [30] M. Yasugaki, K. Itaka, M. Tokunaga, N. Kameda, and T. Tamegai, Magneto-optical observations of crossing-lattice state in $\text{Bi}_2\text{Sr}_2\text{CaCu}_2\text{O}_{8+y}$, *Phys. Rev. B* **65**, 212502 (2002).
- [31] T. Ren, S. Pyon, and T. Tamegai, Growth and characterizations of iron-based superconductor $(\text{Ba}_{1-x}\text{Rb}_x)\text{Fe}_2\text{As}_2$ single crystals, *J. Phys.: Conf. Ser.* **1975**, 012013 (2021).
- [32] M. Terao, Y. Tokunaga, M. Tokunaga, and T. Tamegai, Observation of single vortices by magneto-optical imaging, *Physica C (Amsterdam, Neth.)* **426-431**, 94 (2005).
- [33] R. Prozorov, M. A. Tanatar, N. Ni, A. Kreyssig, S. Nandi, S. L. Bud'ko, A. I. Goldman, and P. C. Canfield, Intrinsic pinning on structural domains in underdoped single crystals of $\text{Ba}(\text{Fe}_{1-x}\text{Co}_x)_2\text{As}_2$, *Phys. Rev. B* **80**, 174517 (2009).
- [34] L. Mei and S.-W. Chan, Enthalpy and entropy of twin boundaries in superconducting $\text{YBa}_2\text{Cu}_3\text{O}_{7-\delta}$, *J. Appl. Phys.* **98**, 033908 (2005).
- [35] T. Ozaki, L. Wu, C. Zhang, J. Jaroszynski, W. Si, J. Zhou, Y. Zhu, and Q. Li, A route for a strong increase of critical current in nanostrained iron-based superconductors, *Nat. Commun.* **7**, 13036 (2016).
- [36] Y. Sun, A. Park, S. Pyon, T. Tamegai, and H. Kitamura, Symmetry-unprotected nodes or gap minima in the s_{++} state of monocrystalline FeSe, *Phys. Rev. B* **96**, 140505(R) (2017).
- [37] C. J. van der Beek, G. Rizza, M. Konczykowski, P. Fertey, I. Monnet, T. Klein, R. Okazaki, M. Ishikado, H. Kito, A. Iyo, H.

- Eisaki, S. Shamoto, M. E. Tillman, S. L. Bud'ko, P. C. Canfield, T. Shibauchi, and Y. Matsuda, Flux pinning in PrFeAsO_{0.9} and NdFeAsO_{0.9}F_{0.1} superconducting crystals, *Phys. Rev. B* **81**, 174517 (2010).
- [38] T. Taen, Y. Nakajima, T. Tamegai, and H. Kitamura, Enhancement of critical current density and vortex activation energy in proton-irradiated Co-doped BaFe₂As₂, *Phys. Rev. B* **86**, 094527 (2012).
- [39] T. Taen, F. Ohtake, S. Pyon, T. Tamegai, and H. Kitamura, Critical current density and vortex dynamics in pristine and proton-irradiated Ba_{0.6}K_{0.4}Fe₂As₂, *Supercond. Sci. Technol.* **28**, 085003 (2015).
- [40] Y. N. Ovchinnikov and B. I. Ivlev, Pinning in layered inhomogeneous superconductors, *Phys. Rev. B* **43**, 8024 (1991).
- [41] S. Kasahara, T. Watashige, T. Hanaguri, Y. Kohsaka, T. Yamashita, Y. Shimoyama, Y. Mizukami, R. Endo, H. Ikeda, K. Aoyama, T. Terashima, S. Uji, T. Wolf, H. von Löhneysen, T. Shibauchi, and Y. Matsuda, Field-induced superconducting phase of FeSe in the BCS-BEC cross-over, *Proc. Natl. Acad. Sci. USA* **111**, 16309 (2014).
- [42] See Supplemental Material at <http://link.aps.org/supplemental/10.1103/PhysRevMaterials.8.084806> for uncompressed polarized-light images resolving twin boundaries within pristine and proton-irradiated FeSe crystals are included.
- [43] M. M. Fang, V. G. Kogan, D. K. Finnemore, J. R. Clem, L. S. Chumbley, and D. E. Farrell, Possible twin-boundary effect upon the properties of high- T_c superconductors, *Phys. Rev. B* **37**, 2334 (1988).
- [44] A. Abrutis, J. P. Sénateur, F. Weiss, V. Kubilius, V. Bigelyte, Z. Saltyte, B. Vengalis, and A. Jukna, Thin YBCO films on NdGaO₃ (001) substrates grown by injection MOCVD, *Supercond. Sci. Technol.* **10**, 959 (1997).
- [45] R. Arpaia, E. Andersson, A. Kalaboukhov, E. Schröder, E. Trbaldo, R. Ciancio, G. Dražić, P. Orgiani, T. Bauch, and F. Lombardi, Untwinned YBa₂Cu₃O_{7- δ} thin films on MgO substrates: A platform to study strain effects on the local orders in cuprates, *Phys. Rev. Mater.* **3**, 114804 (2019).
- [46] A. K. Jha, K. Matsumoto, T. Horide, S. Saini, P. Mele, A. Ichinose, Y. Yoshida, and S. Awaji, Tailoring the vortex pinning strength of YBCO thin films by systematic incorporation of hybrid artificial pinning centers, *Supercond. Sci. Technol.* **28**, 114004 (2015).
- [47] J. Albrecht, S. Brück, C. Stahl, and S. Ruoff, Quantitative magneto-optical analysis of the role of finite temperatures on the critical state in YBCO thin films, *Supercond. Sci. Technol.* **29**, 114002 (2016).
- [48] T. Tamegai, T. Taen, H. Yagyuda, Y. Tsuchiya, S. Mohan, T. Taniguchi, Y. Nakajima, S. Okayasu, M. Sasase, H. Kitamura, T. Murakami, T. Kambara, and Y. Kanai, Effects of particle irradiations on vortex states in iron-based superconductors, *Supercond. Sci. Technol.* **25**, 084008 (2012).